Radial Reactor for Trichloroethylene Steam Reforming

F. Craig Moates, Timothy E. McMinn, and James T. Richardson
Dept. of Chemical Engineering, University of Houston, Houston, TX 77204

A ceramic foam radial reactor was used to convert trichloroethylene by steam reforming, using 0.5 wt. % Pt as a catalyst. With a quartz enclosure heated externally by infrared lamps, the inlet temperature to the catalyst bed was low enough to suppress pyrolysis, but high conversions (0.99999 +) were achieved at the exit. Stable operation up to 600 h with a space velocity of 5.6×10^4 h^{-1} was achieved, but reactant breakthrough then occurred, and the catalyst quickly deactivated. Although the deactivated catalyst was regenerated with carbon burning, activity decline was more rapid due to platinum sintering and washcoat degradation. Measured temperature profiles and model calculations indicated a large gradient in the bed and suggested that stable operation could be extended at lower space velocities. Axial temperature profiles were not uniform, since preferential flow occurred in the middle and lower regions of the radial bed. Potential improvements for future designs are suggested.

Introduction

Chlorinated hydrocarbon contamination in the environment originates from waste streams in industrial processes, containers stored at dump sites, and effluents from other remedial methods such as air stripping and regenerated carbon adsorption. Detoxification methods (Keller and Dyer, 1998) depend on the source and concentration of the contamination. The most common techniques are incineration, which is effective but often generates intermediate toxic compounds and has a low public acceptance, and catalytic oxidation, which is cleaner and less expensive, but includes catalyst poisoning (Agarwal et al., 1992). Research in this laboratory demonstrated steam reforming as an attractive alternative to oxidation (Richardson et al., 1996). Steam reforming, an important process for hydrogen and synthesis gas production (Ridler and Twigg, 1989), proceeds through the reactions:

$$CH_4 + H_2O \leftrightarrow CO + 3H_2 \qquad (1)$$

$$\Delta G^o_{r\times n}\,(600°C) = -4.73\ \text{kJ}\cdot\text{mol}^{-1},$$

$$\Delta H^o_{r\times n}\,(600°C) = +223\ \text{kJ}\cdot\text{mol}^{-1}$$

$$CO + H_2O \leftrightarrow CO_2 + H_2 \qquad (2)$$

$$\Delta G^o_{r\times n}\,(600°C) = -6.81\ \text{kJ}\cdot\text{mol}^{-1},$$

$$\Delta H^o_{r\times n}\,(600°C) = -37.1\ \text{kJ}\cdot\text{mol}^{-1}.$$

For chlorinated hydrocarbons, such as trichloroethylene (TCE), the first reaction (Eq. 1) becomes:

$$C_2HCl_3 + 2H_2O \rightarrow 2CO + H_2 + 3HCl \qquad (3)$$

$$\Delta G^o_{r\times n}\,(600°C) = -345\ \text{kJ}\cdot\text{mol}^{-1},$$

$$\Delta H^o_{r\times n}\,(600°C) = +1.74\ \text{kJ}\cdot\text{mol}^{-1}.$$

Chlorocarbon steam-reforming reactions are very thermodynamically favorable and high levels of destruction are possible. Since they are less endothermic than the first reaction (Eq. 1), heat-transfer problems found in conventional steam reforming are not expected.

We studied the catalytic steam reforming of chlorinated alkanes and alkenes (Ortego et al., 1997; Coute et al., 1998; Intarajarang and Richardson, 1999), chlorinated benzenes (Coute and Richardson, 1999a), and polychlorinated biphenyls (PCBs) (Coute and Richardson, 1999b), and confirmed high conversion levels (> 0.9999) at favorable process conditions (temperature: 400–800°C; GHSV: 10^5–10^6 h^{-1};

Correspondence concerning this article should be addressed to J. T. Richardson.
Present addresses of: F. C. Moates, Exxon Research and Development Laboratories, P.O. Box 2226, Baton Rouge, LA 70821; T. E. McMinn, Exxon Chemical Company, P.O. Box 4900, Baytown, TX 77522.

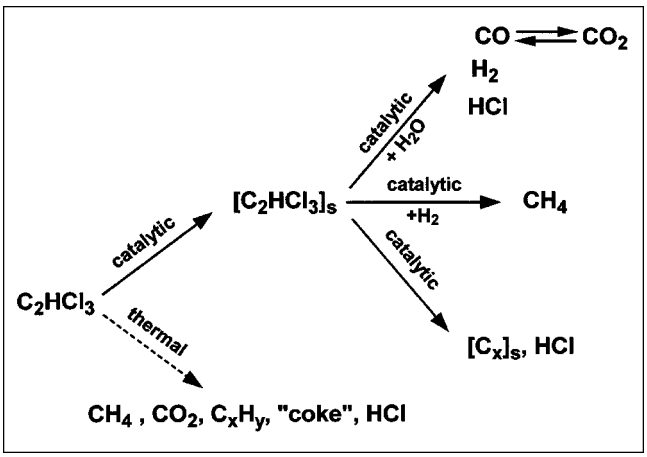

Figure 1. Reaction pathways for the pyrolysis (thermal) and steam reforming (catalytic) of trichloroethylene.

H_2O/C: 5–10). The most active catalysts are supported rhodium, platinum, and palladium, although nickel is an acceptable substitute at higher loadings. This process is suitable for the treatment of effluents from steam-regenerated carbon beds containing a wide range of chlorocarbons or for similar side streams from industrial operations such as vinyl chloride production.

Throughout our research, we encountered difficulties due to thermal pyrolysis via free-radical reactions. These reactions form hydrogen-deficient carbonaceous residues or ''coke,'' quickly deactivating the catalyst and plugging the bed. For example, during kinetic studies (Ortego et al., 1997; Coute et al., 1998; Intarajang et al., 1999; Coute and Richardson, 1999a) conversion decreased rapidly at a rate that increased with both lower conversions and temperatures. This deactivation was eliminated by operation at almost complete conversion and at temperatures above 600–700°C. The reaction pathways for $CHClCCl_2$ steam reforming and pyrolysis are shown in Figure 1. Catalytic steam reforming results in CO, H_2, and HCl, with CO_2 produced via the second reaction (Eq. 2). Hydrogenolysis, which results in CH_4 and HCl, was not often observed, since steam reforming quickly converts CH_4. Catalytic carbon from either decomposition of C-C bonds (cracking) or disproportionation of CO consists of hydrogen-deficient CH_x species that ultimately form carbon. The parallel pyrolysis path gives CO_2, HCl, hydrocarbon intermediates, and ''coke,'' which is primarily a carbonaceous polymer produced by the free-radical reactions. We concluded that these deposits are removed by steam at higher temperatures at a rate that depends on the difference between carbon removal and formation (Ortego et al., 1997).

An effective way of controlling these parallel reactions in laboratory studies was an innovative feed-injection device that minimized preheat and allowed the steam-chlorocarbon feed to contact the catalyst bed at a much lower temperature than the bed itself. In this way, the feed was quickly converted before significant pyrolysis occurred. Any residual carbon formed was removed with steam. Long periods of operation (> 200 h) were maintained without measurable deactivation. However, it was necessary to ensure high conversions. If the conversion decreased by even small amounts (such as from 0.9999 to 0.9980), sufficient unreacted chlorocarbon remained in the bed to cause coking problems.

Although these techniques were successful with small laboratory reactors, they are difficult to imitate with larger reactors. We considered several alternative configurations, and this article reports our experiences with one of these, a radial flow bed constructed of ceramic foam. Radial reactors are common for applications where pressure drop is a consideration (Hlavacek and Votruba, 1977). This is not a problem here—rather, the objective is to create a uniformly heated bed into which relatively cool feed gases can be injected. A radial configuration provides a relatively thin bed in which temperature gradients are minimized. The essential feature, however, is the choice of ceramic foam for the structure of the bed. Reticulated ceramic foams have important properties for catalytic applications (Twigg and Richardson, 1995). These include prefabrication into desired shapes, high thermal stability, low pressure drop, and enhanced heat transfer. Heat transfer is especially important for endothermic reactions, and this has been demonstrated in solar reactor applications (Hogan et al., 1990). Because of their open structure, ceramic foams are especially effective in absorbing radiation to give uniform temperatures throughout the structure. In the current application, heating with infrared radiation promised to satisfy the thermal requirements of the reactor.

In this article, we demonstrate the feasibility of this design for long-term operation and explore the reasons for catalyst deactivation.

Experimental Studies

Radial reactor

Figure 2 shows the shape of the prefabricated, annular structure of α-Al_2O_3 foam obtained from HiTech Ceramics, Inc., and made from 30 PPI (pores per inch) polyurethane foam with random open spherical cells connected together via five or six porelike windows. The average size of the pores is given in Table 1, together with other properties.

The ends of the annular cylinder were sealed with a coating of high-temperature cement and feed gases flowed down the inner section, radially out through the bed, and down the outer space, as shown in Figure 2. A thermocouple well was drilled at the midpoint of the radial segment along the entire length. Bevels at the inner radius of the foam cylinder facilitated sealing the foam to quartz tubing at each end. The lower end of the quartz shell (3-mm thick, 30 cm in length, and 5.7 cm in diameter) was connected to Pyrex tubing, using standard fittings outside the heated zone (Figure 3). A 1-cm ID quartz tube, sealed through the upper closed end of the shell, was beveled to match that at the end of the foam cylinder, and the two were cemented together with high-temperature ceramic cement. A quartz feed tube (1 cm OD, 3 mm wall thickness, and 10 cm in length) was closed at one end and attached to a 25-cm tube with the same diameter. The lower 9 cm of the feed tube had 630 uniformly spaced 0.15-mm holes, pierced with a laser (Laser Cuts Inc.) and positioned to match the inlet of the radial bed. This feed tube was inserted into the foam cylinder through the upper quartz tube emerging from the shell, and the two connected with standard cou-

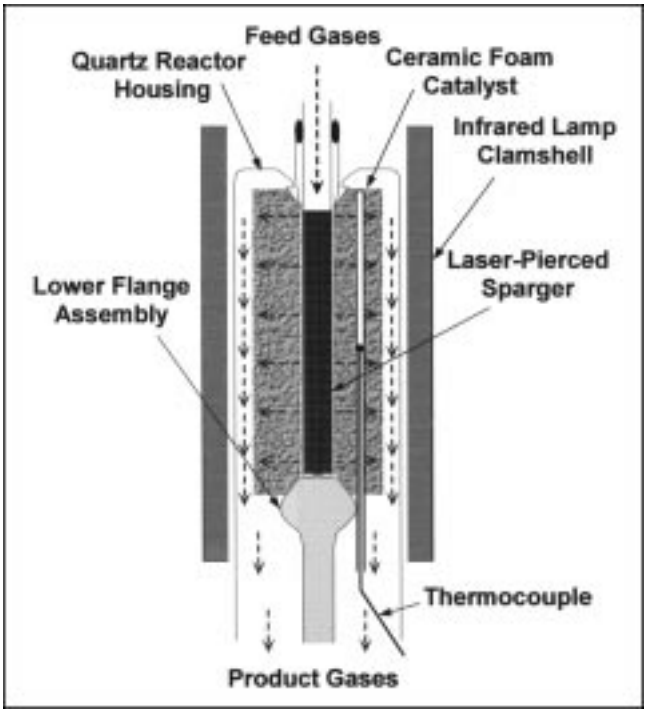

Figure 2. Radial reactor made of ceramic foam.

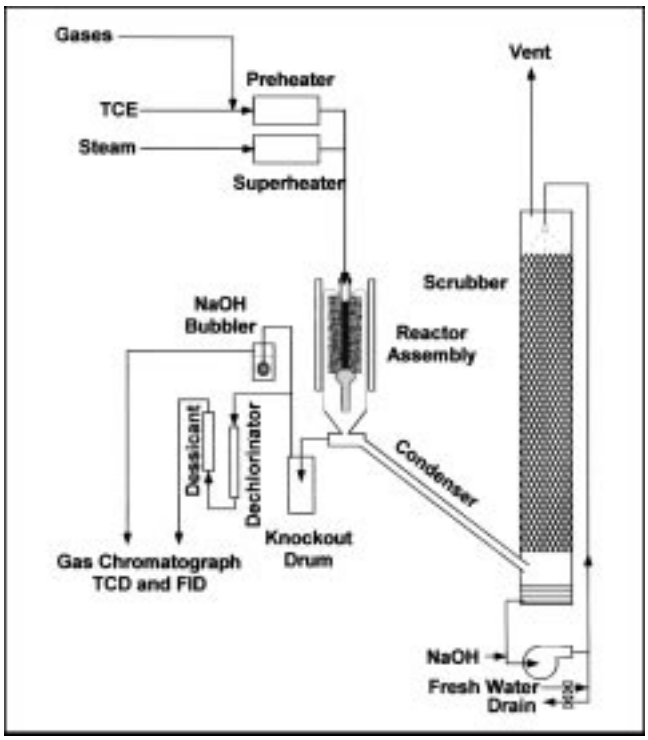

Figure 3. Process flow system.

plings, using Teflon ferrules and Viton O-rings outside the reaction zone. The bed was kept in this position by a 1-cm-diameter quartz rod, beveled to match the foam cylinder and cemented to it.

Infrared lamps around the assembly provided counterflow radiant heating, with a 3-mm quartz-sheathed thermocouple in the well used for feedback control. The reactor shell was resistant to corrosion by wet HCl and had high transparency to infrared energy. The infrared furnace (Research Incorporated Model E4-06) had a maximum output of 5 kW and gave temperatures in excess of 1,000°C.

Process and control system

The overall process system is shown in Figure 3, and details are given elsewhere (Moates, 1997). Gas flows (H_2, He, Ar, and N_2) were regulated by mass-flow controllers (Tylan FC200) in the range 0–200 std. cm^3 per min. Steam flows from 1,000 to 15,000 std. cm^3 per min were generated with a boiler (Reimers JR-1500W), and steam superheated to 300°C with a tubular furnace. A model chlorocarbon, pure trichloroethylene (Aldrich 79-01-6, 99.5%), was injected as a liquid at specified rates with a micropump (SciLog Expert), mixed with a flow of N_2 diluent, and vaporized in a still to assure steady flows of TCE of from 100 to 300 sccm. Temperatures were kept below 250°C to minimize thermal degradation of the TCE. This stream was mixed with the steam flow and passed into the reactor at controlled rates. All lines were electrically heated and insulated.

Table 1. Properties of the Ceramic Foam Radial Reactor

Material	92% α-Al_2O_3, 8% mullite
Length	10 cm
Outer diameter	3.8 cm
Inner diameter	1.27 cm
Average pore size*	0.759 mm
Bulk density*	0.66 g/cm^3
Bulk porosity*	83%

*Provided by HiTech Ceramics, Inc.

Excess steam in the effluent was condensed and scrubbed in a unit packed with polyethylene Pall rings. A spray nozzle at the top of the packing provided fluid recirculation countercurrent to the gas vent, and acid collected in the moisture trap was neutralized with 50 wt. % NaOH solution.

Analytical system

An analytical stream was taken from a small side arm downstream from the condenser after additional moisture removal with a knockout vessel. This stream was split for analysis with separate chromatographic columns and detectors. The stream to the thermal conductivity detector (TCD) was treated to remove chlorinated components and trace amounts of moisture. Acid gas in the flame ionization detector (FID) stream was absorbed in a bubbler containing NaOH solution. Gases were injected into the chromatograph (Perkin-Elmer Sigma 2000) using a 200-μL loop for the TCD and a 3-cm^3 loop for the FID. The large loop was used to approach the lower detection limits needed for TCE measurements.

The FID analyzed for TCE and CH_4 (N_2 carrier Supelco 80/120 Carbopack B-SP1500 column) and the TCD for CO, CO_2, CH_4, H_2, and N_2 (He carrier, Supelco 60/80 Carboxen 1000 column). The constant N_2 flow was used as a reference to obtain product flows, except for HCl, which was calculated from the mass balance. Since CH_4 was measured by both de-

tectors but was not produced in the reactions, a small calibrated flow of CH_4 ($\sim$5 mol %) was introduced into the analytical stream before it was split to serve as a normalizing standard for the two detectors. This, together with the known N_2 flow detected by the TCD, enabled product flows to be determined.

Analytical precision was $\sim$3% for each component. The average carbon balance was $\sim$96%, and H_2 concentrations averaged $\sim$15% above those predicted by stoichiometry. Hydrogen-detection precision was the most uncertain, due to the nonlinear response in the carrier gas.

Throughout this and previous research, no intermediate products of incomplete conversion were detected. This is in agreement with high-precision mass-spectrometry measurements reported by others (Nimlos and Milne, 1992).

Data acquisition

A Keithley-Metrabyte Metrabus system and a 486 computer were used for control and data acquisition. Automatic operation of all devices and data acquisition of flow rates, temperatures, analysis, and so forth, were achieved using interfaces linked to control devices.

Preparation of the foam-supported catalyst

A high surface area washcoat was applied to the foam using a slurry of boehmite and α-Al_2O_3 particles in an acidic suspension. The foam structure was immersed in the washcoat slurry, drained of excess slurry by spinning along its axis, and calcined in air at 600°C for 1 h. This procedure was repeated 4 to 5 times until a uniform washcoat loading of about 10 wt. % was achieved. The foam structure was then soaked in a well-stirred solution of chloroplatinic acid containing just enough platinum to give 0.5 wt. % total metal loading, or 5 wt. % based on the active washcoat. The support was removed after 2 h, drained, and dried in a microwave oven for 5 min, using a rotating device to avoid angular nonuniform migration of the solution. The catalyst was calcined in air at 600°C for 1 h and the process repeated using the original solution. This solution was colorless after 3–4 cycles, indicating that all the platinum had been depleted through adsorption on the catalyst, and the weight change of the dry, gray catalyst corresponded to an uptake of 0.5 wt. % Pt.

Catalyst characterization techniques

Auxiliary catalyst characterization techniques included BET surface area (Quantachrome Quantasorb), *in situ* H_2 chemisorption, X-ray diffraction (Siemens 5000), and electron microprobe analysis (Jeol Superprobe). Fresh and used foam catalyst samples were examined, together with specimens of 5 wt. % Pt loaded onto washcoat particles prepared in a similar manner.

Computational Model

The purpose of the computational model was to estimate temperature profiles in the catalyst bed to aid in the interpretation of experimental data. The following simplified 1-D mathematical model was used to predict temperature and concentration profiles in the radial reactor. Hlavacek and Votruba (1977) have discussed the adequacy of pseudohomogeneous 1-D models for radial reactors, and, in view of the lack of detailed temperature profile measurements in this work, more elaborate models were not justified.

Equations

Conservation equation:

$$\frac{d}{dr}\left(k_s(1-\epsilon)\frac{dT_s}{dr}\right)+h_v(T_f-T_s)-(R_1\Delta H_{R_1}+R_2\Delta H_{R_2})=0, \tag{4}$$

where r is the radial dimension, k_s the solid-bed thermal conductivity, ϵ the total foam-bed voidage, T_s the solid-phase temperature, T_f the gas-phase temperature, h_v the volumetric heat-transfer coefficient, and R_1, ΔH_{R_1} and R_2, ΔH_{R_2} the rate and reaction enthalpies of the reforming and shift reactions, respectively. The volumetric heat-transfer coefficient correlation (Younis and Viskanta, 1993) was

$$h_v=\left(\frac{0.456\,Re^{0.7}}{d_{\text{pore}}^2}\right)k_f, \quad 50<Re<266, \tag{5}$$

where d_{pore} is the average pore diameter of the foam, k_f the thermal conductivity of the foam material, and the Reynolds number is

$$Re=\frac{d_{\text{pore}}U_f\rho_f}{\mu_f}, \tag{6}$$

where the gas density ρ_f is determined from the individual components and viscosity μ_f is that of steam. The interstitial gas velocity, U_f is given by

$$U_f=\frac{1}{\epsilon A_{cs}}\frac{RT_f}{P_{\text{atm}}}\sum_i N_i, \tag{7}$$

with R the gas constant, P_{atm} the reactor pressure, A_{cs} the cross-sectional area for flow, and N_i the molar flow rate of component i.

Gas-phase energy conservation:

$$\rho_f C_{pf}U_f\frac{dT_f}{dr}=h_v(T_s-T_f), \tag{8}$$

where C_{pf} is the specific heat of steam.

Enthalpy of reaction:

$$\Delta H_{R_i}=\sum_{\text{products}}\upsilon_{ji}h_j-\sum_{\text{reactants}}\upsilon_{ji}h_j, \tag{9}$$

where h_j is the enthalpy of formation for compound j, i is the reaction index (reforming or shift), and υ_{ji} the stoichiometric coefficient of component j in the reaction scheme.

Overall species balance:

$$\frac{1}{A_{cs}}\frac{dN_i}{dr}=\pm(\upsilon_{i1}R_1+\upsilon_{i2}R_2), \tag{10}$$

where N_i is the molar flow rate of component i. The specific reaction rate for the reforming step is given by

$$R_1 = (1-\epsilon)\rho_s L_m D_m k P_{TCE}, \tag{11}$$

with ρ_s is the foam density, L_m the fractional metal loading, D_m the metal dispersion, and P_{TCE} the partial pressure of TCE. Pseudo-first-order rate dependence for TCE and the temperature dependence of rate constant, k, was found in previous work (Intarajarang and Richardson, 1999). The shift reaction rate was determined by calculating the change required after reforming to reach equilibrium. This was an oversimplification, since it was previously known that equilibrium is not achieved in the presence of HCl until after very long contact times. Carbon dioxide predictions in the model are high at low conversions, but will be realistic at high conversions, that is, at the outlet of the bed.

For boundary conditions, the feed gas temperature was given as $T_f = T_{fi}$, where T_{fi} is the temperature of the gas at the inlet. The inlet gas component rates were defined by $N_j = N_{ji}$, where N_{ji} is the molar flow rate of component j at the inlet. Another boundary was the control, where $T_{s,k} = T_{s,\text{meas}}$, where $T_{s,\text{meas}}$ is the temperature measured at the midpoint position in the thermocouple, which is well situated at the center of the radial-bed segment, and this was used as the convergence criteria. The convergence adjustment was the heat flux, Q, to the outer boundary of the catalyst, or

$$\frac{dT_s}{dr} = \frac{Q}{k_s}. \tag{12}$$

The equations were discretized with respect to the radial dimension to form a finite-element grid, with tighter spacing through the first 25% of the bed where rapid changes occurred with respect to radial position. With an initial guess for the temperature at the inner boundary of the foam bed, calculations proceeded until they reached the point at which convergence was required (grid element for $T_{s,\text{meas}}$). The calculation was repeated with a correction to the initial temperature guess that was proportional to the deviation in $T_{s,k}$ at the control point from $T_{s,\text{meas}}$. This process was repeated until the system converged in about 20 iterations to within 0.1°C.

Results and Discussion

Measured temperature profiles in the reactor

Temperature profiles in the foam bed reflect heat transfer and homogeneity of flow patterns. Since we did not wish to disturb these patterns in such a small structure, we could not measure precise profiles by placing thermocouples throughout the bed. However, it was possible to measure the axial temperature distribution in the quartz control well (situated in the middle of the annular bed) and the feed tube by maintaining a fixed power input into the infrared lamps and sliding thermocouples down the tubes.

Figure 4 shows these temperature profiles measured at 2-kW input power and with an air flow of 15,000 std. cm^3 per min, which was the highest flow used. In the absence of flow, the feed tube profile was remarkably constant at 924 ± 27°C along the feed tube and the catalyst-bed thermocouple well, indicating uniform heating from the infrared furnace. There was a decrease of about 575°C over the middle center 60% of the feed tube length, so the cooling effect of the incoming gas flow was dramatic. Temperatures were higher at each end, most probably due to incident energy radiation through the sealed ends. A depressed profile was also seen at the center of the radial bed, amounting to a difference of almost 200°C between the middle and both ends of the structure. Since heating throughout the bed was uniform, this was attributed to differences in cooling rates due to inhomogeneities in the flow pattern, so it follows that the gas flow increased in the middle and bottom parts of the bed. The gas did not flow ideally in a uniform radial direction, but was deflected by stagnant regions at each end toward the center of the bed.

These inhomogeneities made it difficult to validate the radial temperature profiles predicted by the model. Figure 5 shows the profile predicted for a flow of 15,000 std. cm^3 per min with the control point (the middle of the thermocouple well) set at 700°C. The calculation assumed uniform radial flow throughout, which was obviously not true. If the average temperatures in the radial-bed center and feed tubes are included in Figure 5, however, these average temperatures match the computed profile well. This indicates that the 1-D model is sufficiently accurate for its purpose, that is, to predict average profiles at this flow rate.

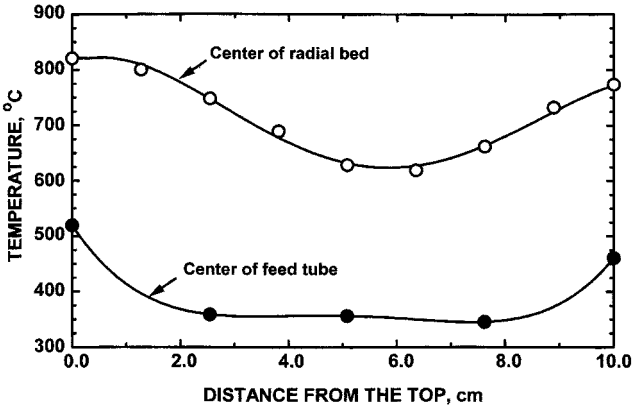

Figure 4. Axial temperature profiles at 2-kW input power and 15,000 std. cm^3 per min flow of air.

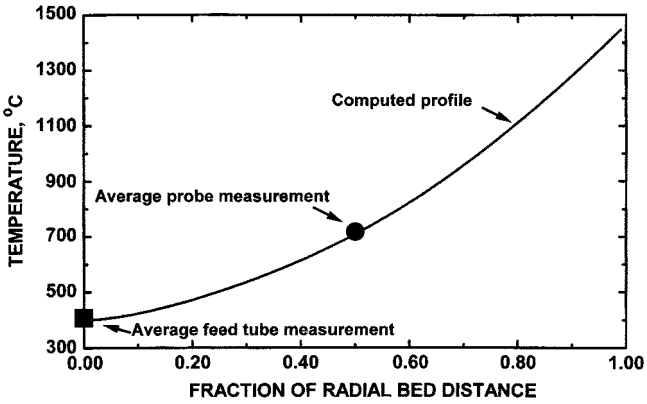

Figure 5. Center radial temperature profile predicted by the model for 15,000 std. cm^3 per min of steam flow with the control point set at 700°C.

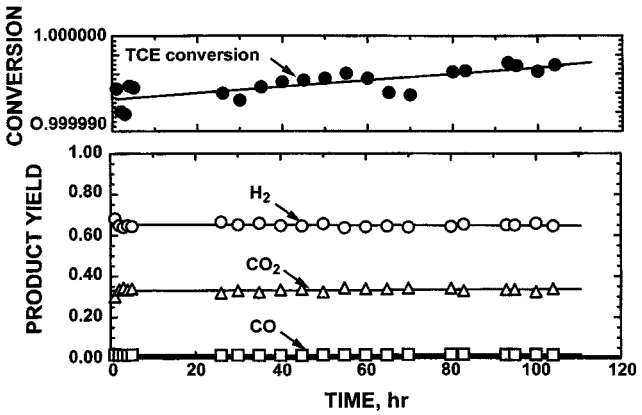

Figure 6. Conversion of TCE in the radial reactor, control temperature = 700°C, $H_2O/C = 25$, steam flow rate = 5,000 std. cm^3 per min.

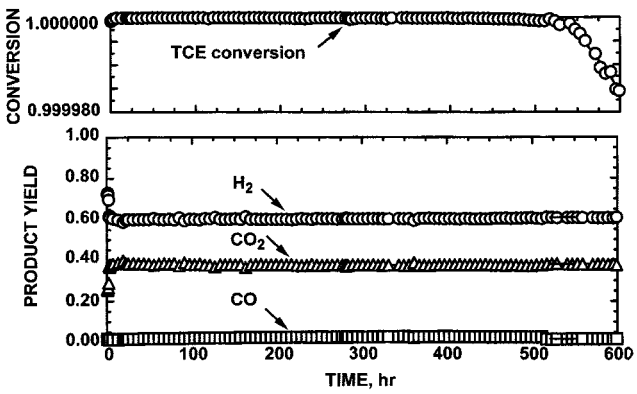

Figure 7. Long-term test of the radial reactor, control temperature = 700°C, $H_2O/C = 25$, steam flow rate = 5,000 std. cm^3 per min.

The profile in Figure 5 shows very high temperatures in the outer section of the radial bed. This was a consequence of the extra power necessary to maintain the control point at 700°C under these high flow conditions. Since temperatures this high are very detrimental to the washcoat and metal crystallites, other strategies are required for high-flow studies. Possibly, the control point should be set to lower temperatures. Better flow homogeneity may be possible by using a ceramic foam with a higher pore density that offers more flow resistance. However, this could also change the energy absorption properties of the bed.

Reactor performance

The principal objective of this research was to test the long-term performance of the radial foam reactor for chlorocarbon-reforming. Figure 6 shows the results of an initial experiment carried out for a period of 105 h. The catalyst was reduced in H_2 at 600°C for 3 h, and the control temperature set at 700°C. A high value of H_2O/C (25) was used to minimize carbon formation from pyrolysis that would otherwise complicate interpretation of the results. Although the model had not been validated for a flow rate of 5,000 std. cm^3 per min due to the nonavailability of measured profiles, the predicted profile indicated a gradual increase from 513°C to 1,005°C for the inner to the outer parts, respectively. This suggests a more uniform flow and lower temperatures at the foam exit.

Conversion of TCE was initially 0.999993 and gradually increased with time. This was probably due to incomplete reduction at the beginning of the run. Product yield was almost constant, although precise examination revealed that the CO/CO_2 selectivity increased from 0.046 to 0.052 during the run. No appreciable change in performance was observed, and the stability of the process was clearly demonstrated over this period. Inspection of the catalyst at the end of the experiment revealed carbon formation near the inlet area of the foam along the entire length, but this carbon deposition did not influence overall performance, since large amounts of uncontaminated bed remained. An identical experiment was conducted for 150 h, with results (not shown here) within 10% of those in Figure 6.

In a more extensive test with a fresh catalyst and identical process conditions (Figure 7), the initial conversion was 0.999999+ and remained constant until about 450 h, when a very slight apparent loss of activity was detected. This continued until about 500 h, when a much faster decrease was observed. Although the product yield remained approximately unchanged, there was a slight loss in the shift activity as the CO/CO_2 ratio increased from 0.035 to 0.065. A similar decrease in shift conversion was observed in previous research (Intarajarang and Richardson, 1999) and was attributed to poisoning by the HCl produced in the reaction. The effect, however, was larger, since the catalyst beds used in those studies were smaller. Inspection of the foam after the 600-h experiment revealed heavy carbon formation throughout the internal portions of the structure and extending past the outlet at certain points.

Figure 8 shows model composition predictions for these conditions. There is a gradient of 500°C across the catalyst bed and complete conversion is not predicted until about 60% of the distance into the bed. Measured exit yields are shown in Figure 8 for comparison, and they are very close to those predicted by the model. Concentration profiles within the bed are not known, so it was not possible to validate the model for accuracy, but the profiles appear reasonable.

Electron dispersive spectroscopic imaging of the inner region of the catalyst foam used in the experiment described earlier showed a washcoat thickness of approximately 100 μm. Platinum dispersed in the support material appeared as small dark spots, and there was a very low chlorine content of 0.07 wt. %, a level comparable to that of the fresh support material. Similar results were found within the outer region, indicating that high levels of chlorine do not accumulate within the catalyst during steam reforming. There were Pt-rich areas on the surface of the outer region, suggesting that sintering of the metal crystallites had occurred. The washcoat had a cracked appearance, possibly due to long-term exposure to the extreme thermal conditions near the bed outlet. In fact, there were indications of fusing with the α-Al_2O_3 understructure.

Separate BET surface-area measurements of the washcoat material itself indicated 90 $m^2 \cdot g^{-1}$, and X-ray diffraction analysis showed a broad pattern of θ-Al_2O_3. The BET sur-

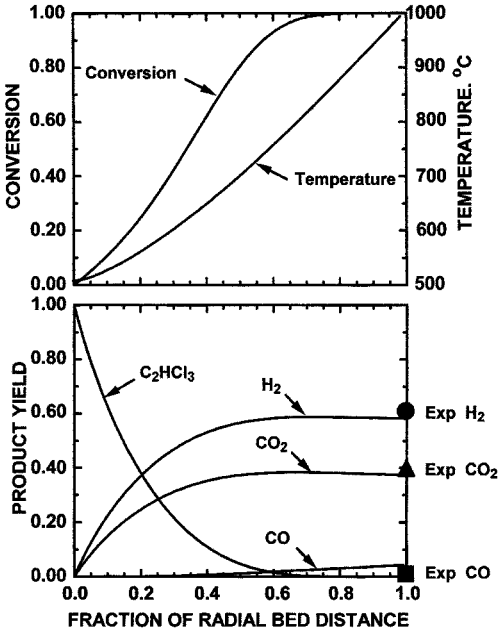

Figure 8. Model predictions of initial radial conversions, temperatures, and product yields for the conditions in Figure 7.

face area increased to 96 $m^2 \cdot g^{-1}$ after calcination at 600°C and then decreased to 84 $m^2 \cdot g^{-1}$ upon heating in air at 800°C for a period of 10 h. Further exposure to 900°C resulted in an additional decrease to 75 $m^2 \cdot g^{-1}$ at 10 h and 68 $m^2 \cdot g^{-1}$ after 125 h, indicating a gradual transition to a lower-area phase. X-Ray diffraction analysis indicated that the washcoat material was exclusively α-Al_2O_3 after heating in air at 1,000°C for 40 h.

Samples taken from the inner and outer regions of the catalyst foam structure were examined before and after removing carbon with air at 600°C. The BET surface area of the inner foam–washcoat composite sample was 5.1 and 8.8 $m^2 \cdot g^{-1}$ before and after oxidation, respectively. Carbon deposition prior to removal was approximately 10 wt. %, which corresponded to 0.23 mol % of the carbon fed to the reactor during the course of the experiment. The increase of the surface area with oxidation was possibly due to removal of this occluding coke. However, the BET surface area of the outer sample only dropped from 7.2 to 6.7 $m^2 \cdot g^{-1}$ upon oxidation, indicating little or no carbon formation. After correcting for the amount of washcoat ($\sim$10 wt. %), this suggests that the inner regions of the washcoat material on the foam structure maintained a surface area of approximately 88 $m^2 \cdot g^{-1}$ (washcoat), while the outer regions decreased to approximately 70 $m^2 \cdot g^{-1}$ (washcoat) in the hotter regions. This is consistent with the separate measurements on the washcoat material and the temperature profile predicted by the model.

During the course of the 600-h experiment, considerable changes occurred that affected the activity of the catalyst in different regions of the bed. Carbon formation was observed in the inner part, while sintering and possible catalyst degradation was suspected in the outer region. While it is impossible at this point to account for these changes in the activity profile of the model, a qualitative description of progressive deactivation suggests itself. Initially the reaction zone (region for complete conversion) is relatively short and high conversions are easily attained. However, since the catalyst bed is exposed to unconverted TCE in this region, carbon deposition occurs and the catalytic activity decreases. This drives the reaction zone deeper into the bed. Although the regions closer to the outer surface are undergoing sintering and other changes, the temperatures are higher and complete conversion is still maintained. Finally, these factors all combine until at about 500 h the reaction zone reaches the outer edge and breakthrough occurs. At this point, deposition of carbon is so extensive that an accelerated deactivation takes place, as evident in the final portion of the conversion curve in Figure 7.

Deactivation–regeneration cycles

The features discussed in the previous section were examined in an experiment in which deactivation was deliberately induced. The feed was a mixture of technical and electronic-grade TCE that was distilled before use to remove heavy residues and reduce the level of impurities (0.5% metals and epoxide stabilizers), which could enhance carbon deposition. Steam flow rates of 15,000 std. cm^3 per min were used to lower conversion and accelerate deactivation.

The experiment was conducted in three phases. In the first, the reaction proceeded at a control temperature of 700°C for 48 h. At this point, the feed flow was discontinued and the catalyst cooled in N_2 to room temperature. The reactor was purged with air and the temperature increased to 600°C to burn off any carbon formed. This was followed by cooling in N_2 to room temperature and reduction at 600°C for 5 h in H_2. The reactor was again purged with N_2 to remove any adsorbed H_2 and cooled to room temperature.

A series of H_2 chemisorption measurements of Pt dispersion was performed *in situ* within the reactor by pulsing H_2 from a 3-cm^3 sample loop into an argon carrier stream every 6 min. The pulses were detected by the TCD to give the amount of H_2 adsorbed on the catalyst in successive pulses, and the dispersion calculated assuming 0.5 wt. % of Pt and a surface Pt/H ratio of unity. These measurements were repeated 3–4 times, with purging of adsorbed H_2 between each measurement.

Following dispersion measurements, the reactor was returned to the operating temperature of 700°C in 50/50 flow of N_2 and H_2 and the reactants reintroduced for the second phase of the experiment. This lasted another 48 h, at which point the previous sequence of steps was repeated. The third phase ended after 110 h of cumulative operation, when carbon formation was observed downstream from the reactor.

Results of this experiment are shown in Figure 9. Initially, complete conversion was not attained and there was a gradual decrease with time. After 48 h, the Pt dispersion after carbon removal had decreased from the initial value of 0.301 to 0.129. At the beginning of phase 2, the conversion did not return to the original value, in contrast to phase 3. However, conversion decreased rapidly after a stable period in phase 2, indicating breakthrough. After removal of carbon in phase 3, the dispersion decreased to 0.058, but conversion increased to the original value. However, deactivation in the breakthrough mode started immediately. Apparently, when the Pt

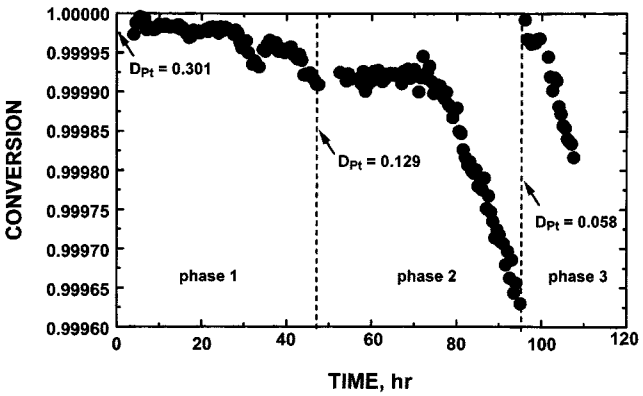

Figure 9. Deactivation–regeneration cycles, control temperature = 700°C, $H_2O/C = 25$, steam flow rate = 15,000 std. cm^3 per min.

dispersion decreased by a factor of about 2, there was sufficient activity within the bed to give stable operation for an additional 24 h. The failure to reach the original conversion could be due to an incomplete regeneration, that is, some carbon remained. At the beginning of phase 3, the dispersion decreased by a factor of 6, yet the catalyst bed was still active enough to give complete conversion. However, subsequent deactivatioin occurred at the same rate as in phase 2. This type of behavior indicates irreversible activity loss, that is, deactivation due to carbon formation is recovered but the effect of dispersion loss is irreversible.

Model calculations at 15,000 std. cm^3 per min confirmed that temperatures in excess of 1,000°C could be expected in the outer regions of the foam bed, thus accounting for the rapid loss of dispersion due to Pt sintering or interaction with the support. More comprehensive results on these deactivation mechanisms will be reported in future publications. These results emphasize the importance of keeping every portion of the bed below 1,000°C for long-term stable operation and suggest that lower space velocities are desirable.

Conclusions

This research demonstrated that a radial reactor made of a washcoated ceramic foam, loaded with 0.5 wt. % Pt and heated externally with infrared lamps, is an effective device for destroying TCE with steam reforming. This configuration should be equally effective with other chlorinated hydrocarbons. The catastrophic deposition of carbon from parallel pyrolysis reactions found in preheated packed-bed tubular reactors was not observed. The reactor gave conversions of 0.999999+ for up to 500 h at a GHSV of 5.6×10^4 h^{-1}. At this point, breakthrough of unconverted trichloroethylene occurred and activity declined rapidly. Observations at 100 and 600 h indicated an increasing amount of carbon deposition moving toward the outer surface. Studies at more severe conditions revealed that the activity could be returned by burning in air and confirmed that deactivation was caused by carbon deposition.

Radial temperature profile measurements at high-flow conditions (GHSV = 1.7×10^5 h^{-1}) showed a large gradient of 700–1,000°C due to the cooling effect of the gas, in agreement with a 1-D model that also predicted more stable operation with lower space velocities. Axial temperature profiles showed pronounced end effects from a nonuniform flow pattern that favored the middle and lower parts of the radial reactor. We conclude that longer and perhaps denser foams would give more uniform radial flows and better performance, but this remains to be confirmed. Foam materials with higher thermal conductivities and radiation adsorptivities (such as SiC) could lead to further improvements.

Although heavy accumulations of carbon were removed with burning, the Pt catalyst lost surface area during the run. This resulted in irreversible deactivation, and the activity of the regenerated catalyst defined faster than before. Such permanent loss of activity may be due to sintering of Pt crystallites or to encapsulation of the metal by the washcoat.

Acknowledgments

This research was supported by a grant from the Gulf States Hazardous Substances Research Center (Project No. 101UHH3214).

Literature Cited

Agarwal, S. K., J. J. Spivey, and J. B. Butt, "Catalyst Deactivation During Deep Oxidation of Chlorocarbons," *Appl. Catal. A. Gen.*, **82**, 259 (1992).

Coute, N., J. D. Ortego, Jr., J. T. Richardson, and M. V. Twigg, "Catalytic Steam Reforming of Chlorocarbons: Trichloroethane, Trichloroethylene and Perchloroethylene," *Appl. Catal. B: Environ.*, **19**, 175 (1998).

Coute, N., and J. T. Richardson, "Steam Reforming of Chlorocarbons: Chlorinated Aromatics," *Appl. Catal. B: Environ.*, in press (1999a).

Coute, N., and J. T. Richardson, "Steam Reforming of Chlorocarbons: Polychlorinated Biphenyls," *Appl. Catal. B. Environ.*, in press (1999b).

Hlavacek, V., and J. Votruba, "Steady-State Operation of Fixed-Bed Reactors and Monolithic Structures," *Chemical Reactor Theory, A Review*, L. Lapidus and N. R. Amundson, eds., Prentice Hall, Englewood Cliffs, NJ, p. 369 (1977).

Hogan, R. E., R. D. Skocypec, R. B. Diver, J. D. Fish, M. Garrait, and J. T. Richardson, "A Direct Absorber Reactor/Receiver for Solar Thermal Applications," *Chem. Eng. Sci.*, **45**, 2751 (1990).

Intarajarang, C., and J. T. Richardson, "Catalytic Steam Reforming of Chlorocarbons: Catalyst Comparisons," *Appl. Catal. B: Environ.*, **22**, 27 (1999).

Keller, R. A., and J. A. Dyer, "Abating Halogenated VOCs," *Chem. Eng.*, **105**, 100 (1998).

Moates, C. F., "Intermediate-Scale Studies of a Catalytic Process for Steam Reforming of Trichloroethylene," PhD Diss., Dept. of Chemical Engineering, Univ. of Houston (1997).

Nimlos, M. R., and T. A. Milne, "Direct Mass Spectrometric Studies of the Destruction of Hazardous Wastes: 1. Catalytic Steam Reforming of Chlorinated Hydrocarbons," *Environ. Sci. Technol.*, **26**, 545 (1992).

Ortego, J. D., Jr., J. T. Richardson, and M. V. Twigg, "Catalytic Steam Reforming of Chlorocarbons: Methyl Chloride," *Appl. Catal. B. Environ.*, **12**, 339 (1997).

Richardson, J. T., J. D. Ortego, N. Coute, and M. V. Twigg, "Chloride Poisoning of Water Gas Shift Activity in Nickel Catalysts," *Catal. Lett.*, **41**, 17 (1996).

Ridler, D. E., and M. V. Twigg, "Steam Reforming," *Catalyst Handbook*, 2nd ed., M. V. Twigg, ed., Wolfe, London, p. 225 (1989).

Twigg, M. V., and J. T. Richardson, "Preparation and Properties of Ceramic Foam Catalyst Supports," *Preparation of Catalysts VI*, J. Marteus, B. Delmon, P. A. Jacobs, and P. Grange, eds., Elsevier, Amsterdam, p. 345 (1995).

Younis, L. B., and R. Viskanta, "Experimental Determination of the Volumetric Heat Transfer Coefficient between a Stream of Air and Ceramic Foam," *Int. J. Heat Mass Transfer*, **36**, 1425 (1993).

Manuscript received Apr. 30, 1999, and revision received Aug. 13, 1999.